Modeling the Binding Sites of Anti-Hen Egg White Lysozyme Antibodies HyHEL-8 and HyHEL-26: An Insight into the Molecular Basis of Antibody Cross-Reactivity and Specificity

S. Mohan, Neeti Sinha, and Sandra J. Smith-Gill
Structural Biophysics Laboratory, Center for Cancer Research, National Cancer Institute, Frederick, Maryland

ABSTRACT   Three antibodies, HyHEL-8 (HH8), HyHEL-10 (HH10), and HyHEL-26 (HH26) are specific for the same epitope on hen egg white lysozyme (HEL), and share >90% sequence homology. Their affinities vary by several orders of magnitude, and among the three antibodies, HH8 is the most cross-reactive with kinetics of binding that are relatively invariable compared to HH26, which is highly specific and has quite variable kinetics. To investigate structural correlates of these functional variations, the Fv regions of HH8 and HH26 were homology-modeled using the x-ray structure of the well-characterized HH10-HEL complex as template. The binding site of HH26 is most charged, least hydrophobic, and has the greatest number of intramolecular salt bridges, whereas that of HH8 is the least charged, most hydrophobic and has the fewest intramolecular salt bridges. The modeled HH26-HEL structure predicts the recently determined x-ray structure of HH26, (Li et al., 2003, *Nat. Struct. Biol.* 10:482–488) with a root-mean-square deviation of 1.03 Å. It is likely that the binding site of HH26 is rendered rigid by a network of intramolecular salt bridges whereas that of HH8 is flexible due to their absence. HH26 also has the most intermolecular contacts with the antigen whereas HH8 has the least. HH10 has these properties intermediate to HH8 and HH26. The structurally rigid binding site with numerous specific contacts bestows specificity on HH26 whereas the flexible binding site with correspondingly fewer contacts enables HH8 to be cross-reactive. Results suggest that affinity maturation may select for high affinity antibodies with either "lock-and-key" preconfigured binding sites, or "preconfigured flexibility" by modulating combining site flexibility.

INTRODUCTION

Antibody-antigen complexes, including antibodies against hen egg white lysozyme (HEL), and in particular the antibody HyHEL-10 (HH10), have long served as model systems for understanding the general principles that govern molecular recognition in protein-protein complexes (Davies et al., 1988; Bentley, 1996, 1989; Wilson et al., 1991; Novotny and Sharp, 1992; Kam-Morgan et al., 1993; Smith-Gill, 1996, 1994; Walls and Sternberg, 1992; Essen and Skerra, 1994; Neri et al., 1995; Tsumoto et al., 1996; Shick et al., 1997; Pons et al., 1999; Bahar et al., 1999; Rajpal et al., 1998). The sequences of thousands of antibodies of the IgG class have been determined (Kabat et al., 1991). However, the three-dimensional structures of only a small subset of sequenced antibodies have been determined by x-ray crystallography, but several have been homology-modeled (Anchin et al., 1991; Bassolino-Klimas et al., 1992; Mas et al., 1992; Tanner et al., 1992; Barry et al., 1994; Orlandini et al., 1994; Tenette-Souaille and Smith, 1998; Tenette et al., 1996).

Six β-turns, three each from the heavy and light chains that form the antigen-combining site, i.e., the complementarity-determining regions (CDRs) of the IgG, are referred to as L1, L2, L3, and H1, H2, H3, respectively. The high variability of the amino-acid sequences of these loops is the source of the vast diversity in antigen specificity, but is also the hurdle in homology-modeling their structures. However, these have been shown to adopt structures that can be classified into sets of "canonical structures" (Conte et al., 1999; Chothia et al., 1989; Chothia and Lesk, 1987; Al-Lazikani et al., 1997). The most variable of them, H3, has not been classified yet due to its high degree of structural diversity.

The antibodies HyHEL-8 (HH8) and HyHEL-26 (HH26) share >90% sequence homology with the structurally defined HH10 (see Padlan et al., 1989; Lavoie et al., 1999; and this article, Fig. 1). The three antibodies utilize the same $V\kappa$ germ-line gene; heavy chains HH10 and HH26 use the same germ-line gene, whereas that of HH8 is a different gene of the same V_H family (Lavoie et al., 1999; Smith-Gill et al., 1987). We have shown previously that all three antibodies recognize coincident (essentially identical to that of HH10) epitopes on HEL (see Lavoie et al., 1999, 1992; and this article, Table 1). Among the three antibodies, HH8 is the most cross-reactive, with kinetics of binding that are relatively invariable compared to HH26, which is highly specific and has quite variable kinetics (Lavoie et al., 1999, 1992; Li et al., 2001). Their distinct functional behaviors (Table 1), despite their very high degree of sequence identity, makes this set of antibodies ideal for analysis of the structural parameters that underlie their functional differences.

```
VH
            1           29 30 31 32   35      44   50 51  53  56 58  60      73      78 81 82A 84       94    100 102 105 108
HH10   D----------------|T-S|--------------R-----|Y-V|-|Y|-S--|Y|----------T---------Y----N-------N--|   |-D G D-Y---Q---L----
HH26   E----------------|  |--------------K-----|  |-|I|-----| |----------A----------------------R--| E M |----------S----
HH8    E----------------|I-R|--------------K-----|  |-|I-F|-N--|-F|--------H----S-------------------|   |----T----
```

```
Vk
         1       17        30          49     53        74 75 77        93  96  100
HH10   --------N-------|-G|--------K----|-| |-|-|----S-I--S-----|S|---| |--------
HH26   --------D-------|-S|-------------|-| |-|-|------V--------|  |---| |--------
HH8    --------D-------|  |--------T----|-| |-|T-|--T---T-------|N |---| |--------
```

FIGURE 1 Sequence comparisons. Heavy- and light-chain amino-acid sequences of HH10 (*top row*), HH8 (*middle row*), and HH26 (*bottom row*).

We describe here the homology-modeled three-dimensional structures of HH8 and HH26 complexes with HEL. The recently refined x-ray structures of a fourth antibody in the same family, HH63 (Li et al., 2000), as well as those of HH26 and a recombinant antibody H8L10 (Li et al., 2003), complexed with HEL, show that the complexes are all very similar in structure to each other and to that of HH10, validating the approach of homology-modeling for these complexes. Based on detailed analyses of their molecular structures and interactions, we present a hypothesis for the structural bases of their fine specificity and cross-reactivity differences. The x-ray crystallographic structure of the HH26 complex is now available for evaluation of the homology model, but it is unlikely that a high resolution structure of the

H8-HEL complex will be forthcoming (Li et al., 2003). Therefore, these models provide a valuable tool for comparing the structure-function relationships in these antibodies.

MATERIALS AND METHODS

Overall strategy

The structures of all loops, except H3, were modeled using the coordinates of Fab10-HEL complex structure (PDB 3HFM; Padlan et al., 1989) as template. The coordinates of higher resolution of scFv10-HEL complex (PDB 1c08) were not used because scFv10-HEL has significantly different kinetic and thermodynamic properties from those of Fab10-HEL (Kondo et al., 1999). On the other hand, because numerous studies from our laboratory have demonstrated functional equivalence of the Fab antibody to the IgG antibody, we therefore concluded that the Fab structure would be

TABLE 1 Summary of functional characteristics of anti-HEL antibodies HH8, HH10, and HH26

Characteristic	HH8	HH10	HH26	Reference
Stage of immune response	Hyperimmune	Hyperimmune	Secondary Ab	Mallett et al. (1989); Lipschultz et al. (2000)
"Hot spot" residues in HEL epitope (top 5)*	K97, Y20, G16, W63, D101	K97, Y20, G16, R21, N93	K97, Y20, W63, D101, R21	Kam-Morgan et al. (1993); Li et al. (2001); Pons et al. (1999); and Smith-Gill lab (unpublished data)
Affinity ($K_A, 10^8 M^{-1}$) (HEL, 25°C)	232	43.9	1.50	Lavoie et al. (1992, 1999); Li et al. (2001)
Relative decrease in affinity caused by Ag mutations	Low ($\Delta\Delta G = 0–2$)[†]	Moderate ($\Delta\Delta G = 0.1–4$)	High ($\Delta\Delta G = 0.2–5+$)	Smith-Gill et al. (1984), (1987); Lavoie et al. (1990, 1999)
Relative cross-reactivity with mutant Ag	High	Moderate	Low	Lavoie et al. (1989, 1990, 1999)
Apparent k_{on} ($10^5 Ms^{-1}$) (HEL, 25°C)	1.9	2.3	0.09	Lavoie et al. (1999)
Relative decrease in net k_{on} caused by Ag mutations	Low	Low	High	Lavoie et al. (1999); Li et al. (2001)
Apparent k_{off} ($10^{-4} s^{-1}$) (HEL, 25°C)	0.2	0.5	4.9	Lavoie et al. (1999)
Relative decrease in net k_{off} caused by Ag mutations	Low	High	High	Lavoie et al. (1999)
Binding kinetics	2-step	2-step	2-step	Lipschultz et al. (2000); Li et al. (2001); Mohan and Willson (unpublished data)
Rate limiting step of association	Encounter	Encounter	Encounter/ docking	Lipschultz et al. (2000); Li et al. (2001)
Association step most affected by epitope mutations	Both, but minimally	Docking	Encounter	Li et al. (2001); Sinha et al. (2002); and Smith-Gill lab (unpublished data)
ΔG of association (kcal/mol) (HEL, 25°C)	−13.6	−13.1	−10.5	Lavoie et al. (1992), 1999; Li et al. (2001)
Percent of free energy from docking (HEL, 25°C)	23%	15%	8%	Lipschultz et al. (2000); Li et al. (2001); and Smith-Gill lab (unpublished data)
Relative thermodynamic nature of association	Most entropically driven	Intermediate	Most enthalpically driven	Mohan and Willson (unpublished data)

*Residues contributing the most free energy of binding determined by alanine scanning; alanine mutants of these residues all lost at least 1 kcal/mol compared to binding by respective Ab to unmutated HEL. Order of listing reflects commonality, not magnitude of energy loss.
[†]Range of energy loss (kcal/mol) caused by alanine mutants of epitope contact residues.

a more biologically realistic template for the other antibodies. The conformational space has been sampled to model H3. Available structures of the related antibody complex H63-HEL (Li et al., 2000) and the recently determined structures of HH26-HEL and H8L10-HEL (Li et al., 2003) support epitope mapping results (Li et al., 2001; Lavoie et al., 1999; Smith-Gill et al., 1984), suggesting that the orientation of these antibodies to the lysozyme epitope are essentially identical. Hence, the complexes have been modeled with this assumption, with the antibodies docked to HEL identically as HH10. Only the Fv portions of the antibodies were modeled.

Modeling the complete structure of the complexes involved the following steps:

1. Minimization of the HH10 template structure.
2. Starting with template, framework residues were first mutated to either HH8 or HH26 consensus sequence.
3. Mutations in CDRs L1, L2, L3, H1, and H2 of both HH8 and HH26 were homology-modeled using the program LOOK (Molecular Applications Group, Palo Alto, CA).
4. Models were utilized to further model H3 of the respective antibodies, using the program ICM (Molsoft LLC, Metuchan, NJ).

The program LOOK, Vers. 3.0, was used for the purposes of 1), minimizing the template structure by optimizing the packing interactions through protein side-chain repacking; 2) modeling amino-acid mutations in the framework of template structure to sequences corresponding to either HH8 or HH26; and 3), to mutate and optimize the packing interaction of the side chains of the CDRs. The module Model Mutant, which is based on the algorithm CARA (Lee and Levitt, 1991; Lee and Subbiah, 1991), was used to mutate the framework. The module Model Homology, based on the algorithm SEGMOD (Levitt, 1992, 1983), was used for tasks (1) and (3) (see above). The loop-modeling algorithm in the program ICM (Molsoft, La Jolla, CA), Vers. 2.7, was used alone to model CDR H3 of both HH8 and HH26. The procedure samples the conformational space of backbone and side chains, using a biased-probability Monte Carlo search method (Abagyan and Totrov, 1994), and globally optimizes the energy function consisting of ECEPP/3 and solvation energy terms. All residues of H3 as well as those within a radius of 5 Å of this loop were searched whereas the rest were constrained.

Numbering of residues and CDRs are according to Kabat et al. (1991). Loops that have sequences identical to template were assigned the same backbone conformations as that of the template. For those with identical lengths but different sequences, the template sequence and conformation was initially adopted, upon which "mutations" were carried out using the Model Homology module of the program LOOK, permitting for backbone conformational changes that might be required during the amino-acid substitutions.

The program CHARMM (Brooks et al., 1983), Vers. 24, was used for all minimizations. All-atom force-field set PARAM20.0 was used to assign atomic charges and force fields. A nonbonded cutoff of 9 Å was used with a shifted potential and force-smoothing function. Constant dielectric is used. Either Adopted Basis Newton-Raphson method or steepest-descent minimization algorithms were used for all energy minimizations. The program QUANTA 97 (MSI, San Diego, CA) was used for all other visualizations, calculating hydrogen bonds, nonbonded contacts, contact areas, and for generating most of the pictures. A distance of 4 Å cutoff was used to calculate nonbonded interactions and a probe radius of 1.4 Å used to calculate solvent-accessible surface and contact areas.

Minimization of template structure

Hydrogens were fixed to the x-ray structure and minimized for 100 ABNR steps (using CHARMM) to relieve any short contacts caused by fixing of the hydrogen atoms. This structure was imported into LOOK and a "copy" of the sequence of each chain was made, which is identified as a different molecule. This "copy" was then homology-modeled, using module "Model Homology," with the original x-ray structure as the template to predict side-chain conformations. Hence, the backbone and side-chain positions of the "copy" are adjusted to settle in positions for optimal side-chain packing interactions.

Modeling of HH8/HH10-Japanese quail lysozyme complex

The x-ray structure of Japanese quail lysozyme (JQL) (PDB code: 2IHL) was overlaid on HEL of HH10-HEL (minimized template) complex for best root-mean-square (RMS) fit. Coordinates of JQL and HH10 from this procedure was used to generate HH10-JQL complex. The same was done with HH8-HEL complex to obtain HH8-JQL complex.

RESULTS

Comparison of Fv region sequences of HH8 and HH26 with HH10

The Fv segment of HH8 has ~92% sequence identity with HH10 (Fig. 1) with all corresponding CDRs of identical length. (Note that, although only the Fv segments of the antibodies were modeled here, the word *antibody* is used in the text to denote these models and their complexes.) Five substitutions are found in light chain, of which the only CDR mutation, $S93_{VK}N$, is in L3, and the rest are in framework regions. The H chain of HH8 has 13 substitutions relative to HH10, of which five are in CDRs. Most of the differences are in H2, where four substitutions are found ($V51_{VH}I$, $Y53_{VH}F$, $S56_{VH}N$, and $Y58_{VH}F$). A single substitution is found in H3($D101_{VH}T$). The notable framework substitutions are $K49_{VK}T$, $G49_{VH}E$, and $T30_{VH}I$. Overall, three CDRs (L1, L2, and H1) are identical with the template.

The Fv segment of HH26 has ~94% sequence identity with HH10 (Fig. 1), with 10 amino-acid differences in the H chain and only three in the L chain, with all corresponding CDRs of H26 and H10 of identical length. Of the 10 H chain differences, only three are in CDRs (H2: $V51_{VH}I$; H3: d $D96_{VH}E$; and $G100_{VH}M$), and a notable $N94_{VH}R$ framework mutation. Arginine is found in this position predominantly (Chothia and Lesk, 1987). One of the L chain substitution is in L1 ($G30_{VK}S$) and the rest are in framework regions. Four CDRs (L1, L2, L3, and H1) of HH26 are identical with those of template.

Minimization of template structure

The positions of side-chain atoms beyond the C^{β} atom are not quite reliable in template HH10 complex (PDB 3HFM), solved at 3.0 Å resolution of Padlan et al. (1989). Hence, the structure was minimized for energy by optimizing the packing of side chains as detailed in Methods. This procedure, although not a substitute for a higher-resolution crystal structure, eliminated certain bad contacts and large torsion strains present in the x-ray structure. Total energy of the repacked system is −4970 kcal/mole compared to −4267 kcal/mole of the x-ray structure, with substantial difference in the van der Waals component (−647 kcal/mole, compared to −256 kcal/mole of the x-ray structure). The repacked structure has an RMS difference of 1.04 Å with respect to x-ray structure, with L1 exhibiting the maximum difference

(1.39 Å). A likely reason for this is the change in the backbone dihedral angles (Φ, Ψ) of $G30_{VK}$ from [−79.8, 119], found in x-ray structure, to [−58, −66] in the repacked structure. All the intermolecular nonbonded contacts that were observed in the x-ray structure have been maintained after the repacking.

Modeling of the hypervariable loops

With the exception of H3, all the CDRs were modeled based on the canonical-structures hypothesis (Chothia et al., 1989; Chothia and Lesk, 1987). The four homologous substitutions of CDR-H2 of HH8 were modeled with the program LOOK, as described in Methods. Finally, CDR-H3 of both HH8 and HH26 were modeled using the biased-probability Monte Carlo method (Abagyan and Totrov, 1994) incorporated in the program ICM. The individual steps are described in the following sections.

Models of HH8 loops L1, L2, L3, and H1

The sequences of CDRs L1, L2, and H1 are identical to those of HH10 (Fig. 1). L3 has one homologous substitution ($S93_{VH}N$). CDRs with identical lengths and same critical residues assume canonical structures (Chothia and Lesk, 1987; Anchin et al., 1991; Bassolino-Klimas et al., 1992; Mas et al., 1992; Tanner et al., 1992; Orlandini et al., 1994; Tenette-Souaille and Smith, 1998; Tenette et al., 1996). Therefore the backbone conformations of CDRs L1, L2, L3, and H1 are assumed to be the same as that of the template. Backbone rearrangement to accommodate the $S93_{VH}N$ mutation was modeled using the Model Homology module of the program LOOK (see Methods). Stereoviews of the overlays of the energy-minimized loop models with those of HH10 CDRs are shown in Fig. 2. RMS difference of the CDRs L1, L2, L3, and H1 with respect to the template, considering only C^α atoms, are 0.7 Å, 0.47 Å, 0.54 Å, and 0.4 Å. L1, L2, L3, and H1 have been reported to belong to the canonical classes 2, 1, 1, and 1′, respectively.

Model of HH8 loop H2

Template CDR-H2 was appropriately mutated to those found in HH8, then modeled as a homology protein using the program LOOK. H2 has four mutations compared to HH10 (Fig. 1), with different side-chain volumes and hydrogen-bonding capacities that could influence backbone conformation. The residue 71_{VH} has been noted to have an effect on the conformation of this CDR (Tramontano and Lesk, 1992), and this residue is arginine in all the three antibodies. In HH10, $R71_{VH}$ interacts with its CDR-H2 residue $V51_{VH}$, which is mutated to $I51_{VH}$ in HH8. Therefore, while modeling this loop, necessary freedom for backbone was provided to accommodate the differences in these side-chain volumes.

The final H2 model had an RMS of 1.0 Å (compared to the template structure) considering only the backbone atoms, and 1.5 Å when all the atoms where considered. The substitution $I51_{VH}V$ increases van der Waals interaction with $R71_{VH}$, now oriented closer to H2, with more compact packing with the backbone of $G55_{VH}$ (not shown). The backbone dihedrals of residues 53_{VH} and 54_{VH} have changed to [−64, 96] and [162, −15] from [−54, 157] and [57, 31] , respectively, observed in the template. Values χ_1 and χ_2 of substituted residue $F53_{VH}$ are 180° and 134°, respectively, and are different from 83° and −85° of the corresponding residue $Y53_{VH}$ in HH10. Backbone dihedrals angles (Φ, Ψ) of $F58_{VH}$ are [−130, 95], compared to [−110, 125] of $Y58_{VH}$ in HH10, orienting $F58_{VH}$ slightly away from HEL (Fig. 3). There is a large 1.7 Å positional shift at the C^α atom of $F58_{VH}$, compared to the corresponding position of $Y58_{VH}$. This loop has been classified as belonging to canonical class 1 (Al-Lazikani et al., 1997). However, the hydrogen-bonding pattern of the loop (Al-Lazikani et al., 1997) suggests that this CDR of both HH8 and HH10 might belong to class 2B. The three hydrogen bonds between the main chain atoms of the turn residues 52_{VH}, 55_{VH}, and 56_{VH} (52N-O56, 52O-N55, and 52O-N56) that characterize the canonical class of this CDR are also found in these antibodies. This model of the complex was minimized for energy by 100 steps of ABNR and was used to model H3 in the next step.

Model of HH8 loop H3

CDR-H3 is defined between the residues 95 and 102, according to Kabat and co-workers, and could possess between five and 15 residues (Wu et al., 1993; Kabat et al., 1991). $D101_{VH}T$ is the only substitution in this loop relative to HH10 (Fig. 1). In the HH10-HEL x-ray structure (Padlan et al., 1989), $D101_{VH}$ does not make any contacts with HEL; the residue at position 101_{VH} usually makes only minimal contacts with antigen (MacCallum et al., 1996). In the crystal structure of the HH10 template, there is an electrostatic interaction between the residue $K49_{VK}$ and the aspartic-acid residue at both positions 96_{VH} and 101_{VH}, which might influence the conformation of H3. However, in HH8 both the residues $K49_{VK}$ and $D101_{VH}$ are mutated to threonine, precluding electrostatic interactions. Hence, it was felt necessary to model this CDR rather than assuming the same conformation as the template despite the identity in length. Modeling was carried out using the biased-probability Monte Carlo search method, using the program ICM. The loop H3 of a sugar-binding antibody was recently modeled using this program and was found to successfully explain the experimental observations (Miller et al., 1998).

The lowest-energy model of H3 has an RMS difference of 0.7 Å (with backbone atoms) from H3 of HH10, and has quite a few notable side-chain orientation differences compared to the template. Residues $D96_{VH}$ and $W95_{VH}$ are more solvent-exposed than in HH10. The solvent-accessible area of H3 is
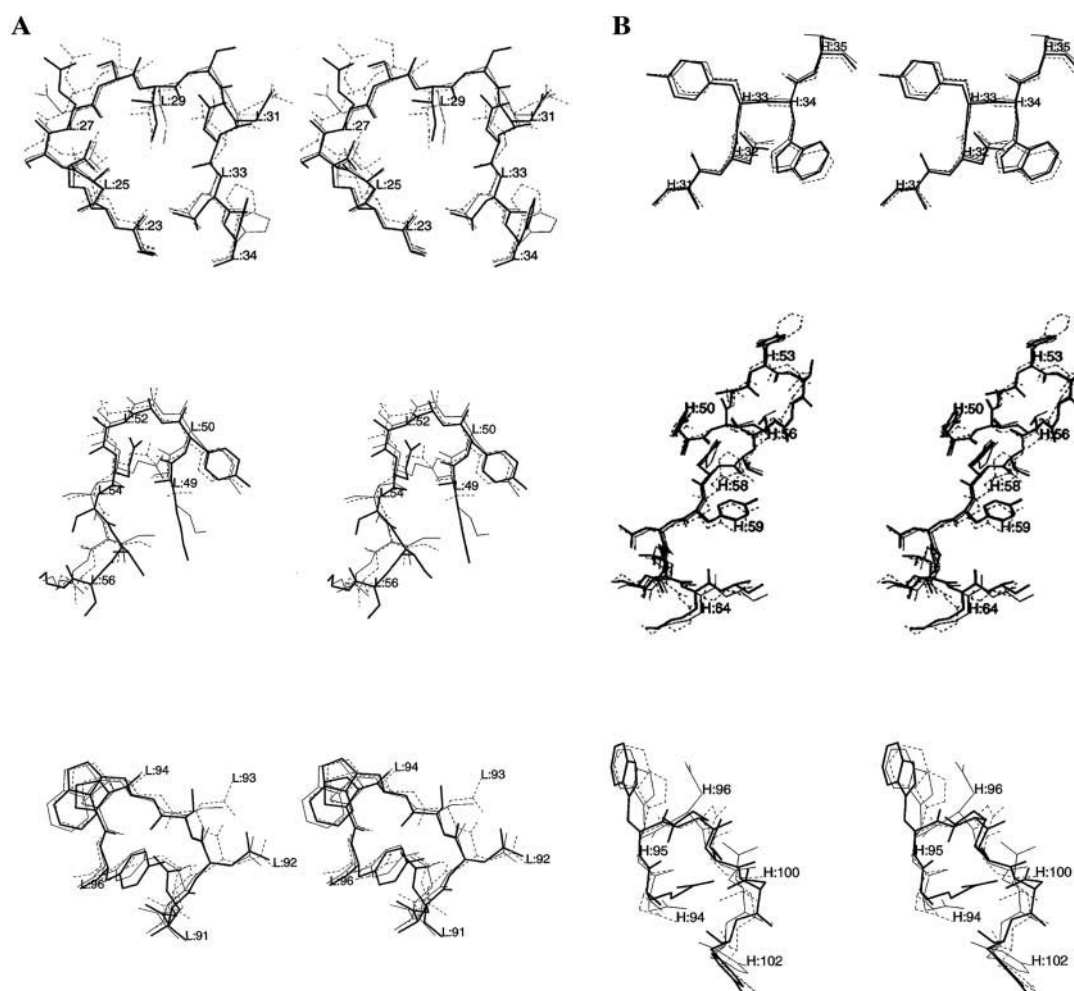
FIGURE 2 Comparisons of CDRs of HH8, HH10, and HH26. (*a*) Overlays of light-chain CDRs of HH8 and HH26 with those of HH10. Stereoviews of light chain CDR residues of HH8 (*dashed lines*) and HH26 (*thick lines*) superposed for best RMS fit on the corresponding HH10 residues (*thin lines*). The top, middle, and bottom rows of figures correspond to L1, L2, and L3 CDRs, respectively. Numbering of residues are according to Kabat et al. (1991). (*b*) Overlays of heavy-chain CDRs of HH8 and HH26 with those of HH10. The top, middle, and bottom rows of figures correspond to H1, H2, and H3 CDRs, respectively. In H2, flipping of HH8 residues 53_{VH} and 58_{VH} with respect to its corresponding residues in HH10 and HH26 may be observed.

44 Å^2. $W95_{VH}$ adopts a different conformation in an earlier instance when HH10 was used as a template to model anti-cystacin antibody (Schiweck and Skerra, 1997). The absence of the electrostatic interactions between D96VH and $K49_{VK}$, now mutated to threonine, could be the reason for the former's altered conformation in HH8. Overlay of the structure of this loop with that of HH10 is shown in Fig. 2.

Models of HH26 loops L1, L2, L3, H1, and H2

The sequences of CDRs L2, L3, and H1 of HH26 are identical to those of HH10 and hence, template conformations were adopted for them. L1 and H2 have a single substitution each, $G30_{VK}S$ and $V51_{VH}I$, respectively. These two substitutions were carried out using the Model Homology module of the program LOOK, where the backbone dihedrals were allowed to relax to accommodate any minor conformational changes that could arise due to the two substitutions. This model was minimized for energy by 100 steps of ABNR before proceeding to the next step for modeling CDR-H3.

Model of HH26 loop H3

There are two substitutions in this CDR: $D96_{VH}E$ and $G100_{VH}M$. The conformational space of the backbone dihedrals were searched by the biased-probability Monte Carlo method described above. The lowest energy structure yielded from the search had an RMS of 1.5 Å with respect to the template, when all the atoms of H3 were considered (Table 2).

Final models of HH8 and HH26 Fv regions

Once H3 was fixed, the models were subjected to energy minimization until the energy gradient was <0.001 kcal/Å.
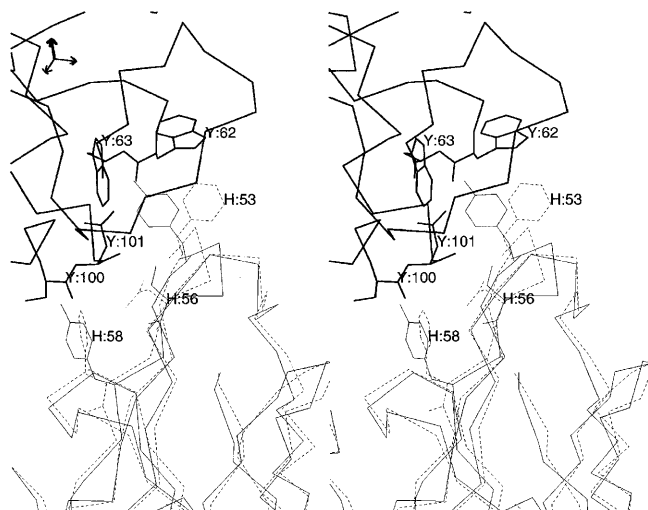
FIGURE 3 Comparison of CDR-H2 of HH8 and HH10. Stereoviews showing the overlays of heavy-chain CDR-H2 of HH8 (*dashed lines*) with HH10 (*thin lines*) and their corresponding contact residues of HEL (*thick lines*). Residues at positions 53_{VH} and 58_{VH} of HH8 are phenylalanines (both are tyrosines in HH10), and are flipped away from HEL, with a substantial backbone conformational change. Due to the change in orientation of phenylanalanine residues with respect to HEL, CDR-H2 of HH8 makes very minimal contacts with HEL. The only hydrogen bond that a H2 residue of HH8 forms with HEL is between $N56_{VH}$ (serine in HH10) and $S100_{HEL}$.

Backbone atoms were not constrained during this step. Energy of the minimized model of HH8 was -4913 kcal/mole, compared to the initial value of -3319 kcal/mole. The final energy of the HH26 model was -4955 kcal/mole (*initial energy* $= -3363$ kcal/mole). Overlays of the final models with the template HH10 are shown in Fig. 4, and RMS differences of the loops with respect to those of HH10 are shown in Table 2. Both modeled structures had overall RMSD of <1 Å from the H10 structure, whether C^{α} or backbone were considered. However, CDR regions of both the antibodies exhibit significant movements. Both antibodies show large (RMS > 1 Å) shifts in CDR-L2 and CDR-H3 with respect to HH10. L2 of HH26 is tightly packed

TABLE 2 Tabulation of RMS differences of modeled HH8 and HH26 structures with respect to HH10 template

	HH8	HH26
All C^{α} atoms	0.67	0.57
All backbone atoms	0.76	0.64
CDR	1.36 (0.95)*	1.01 (0.80)
CDR-L1[†]	1.27 (0.90)	0.90 (0.63)
CDR-L2	1.15 (0.76)	1.76 (1.24)
CDR-L3	0.91 (0.70)	0.70 (0.35)
CDR-H1	0.64 (0.40)	0.42 (0.20)
CDR-H2	1.52 (1.00)	0.60 (0.20)
CDR-H3	1.21 (0.70)	1.52 (1.00)

*RMS differences obtained by superposing all atoms of the backbone as well those of C^{α} alone; the later values are shown within parentheses.
[†]CDRs of heavy and light chain are denoted as H1, H2, H3, and L1, L2, L3, respectively.
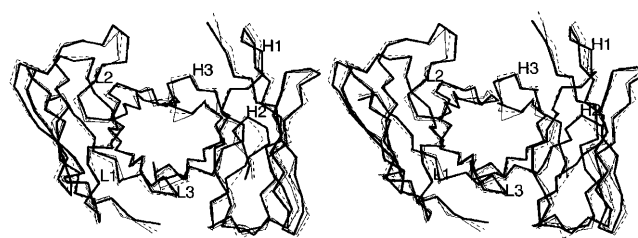
FIGURE 4 Overlays of the entire C^{α} backbone of HH8, HH10, and HH26. Stereoviews of superpositions of the C^{α} traces of HH8 (*dashed lines*) and HH26 (*thick lines*) with HH10 (*thin lines*). Each CDR is labeled and their corresponding RMS with respect to HH10 is tabulated in Table 2.

against its H3, whereas that of HH8 has very minimal packing (Fig. 5), with total area of contact between the residues of L2 and those of H3 in HH26 at 142 $Å^2$ compared to 104 $Å^2$ in HH8. In addition, CDR-L1 and CDR-H2 of H8 showed large shifts. H2 shifts are not unexpected, due to the number of amino-acid substitutions.

Distribution of charged and hydrophobic residues in binding sites

The numbers of hydrophobic and charged residues (seen as *brown*, *blue*, and *magenta* in Fig. 6) vary in each antibody. Among the three antibodies, HH8 has the most hydrophobic residues and fewest charged residues. In contrast, HH26 has the fewest hydrophobic residues and most charged residues. HH10 ranks between the other two antibodies for both of these properties. The increased hydrophobicity of HH8 results from its substitutions in its loop H2 as well as the framework substitutions $K49_{VK}T$ and $T30_{VH}I$. The substitution $N94_{VH}R$ renders the binding site of HH26 more charged.

Intramolecular salt bridges in the Fv region of HH8, HH10, and HH26
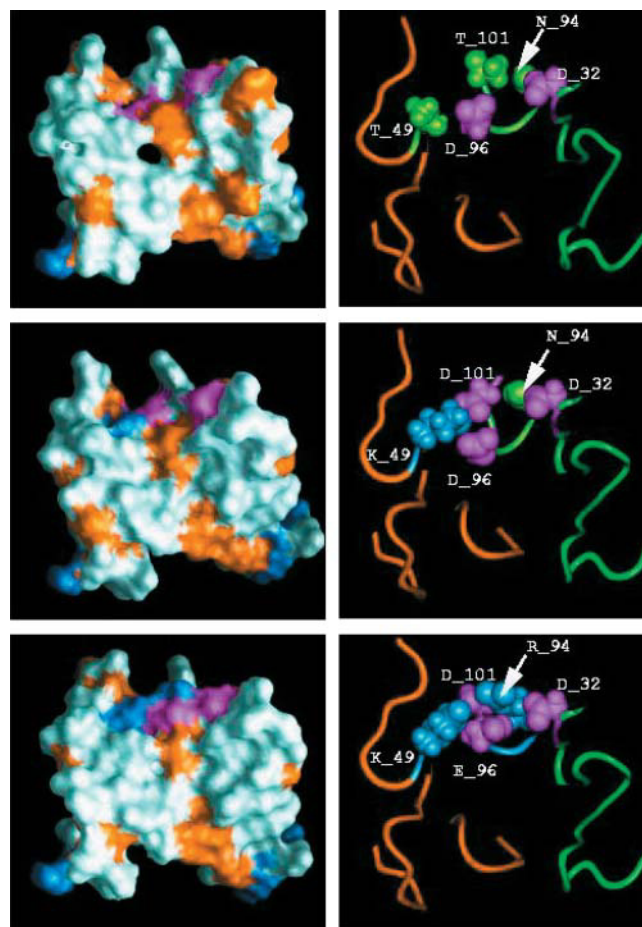
The three Fv vary in the number of intramolecular salt bridges they contain. In their entire Fv regions, HH8 has the fewest (two) (Table 3) and HH26 has the most (eight), whereas HH10 has an intermediate number (five) (Table 3). They can be classified in three different categories, where both the participating residues of the salt bridge belong to 1), light chain, i.e., light-light category (l-l) 2); light and heavy chain, i.e., light-heavy category (l-h); and 3), heavy chain, i.e., heavy-heavy category (h-h). The two salt bridges found in HH8 (l-l: $R24_{VK}$-$D70_{VK}$ and h-h:$K64_{VH}$-$D86_{VH}$) are commonly present in all three antibodies. In both HH10 and HH26 (but not HH8), framework residue $K49_{VK}$ is involved in two l-h salt bridges, each with heavy-chain CDR-H3 residues $D101_{VH}$ and $D/E96_{VH}$ HH10 and HH26, respectively. In HH8, residues 49_{VK} and 101_{VH} are both mutated to threonine, thus precluding the electrostatic interactions between them, and most likely influencing the conformation
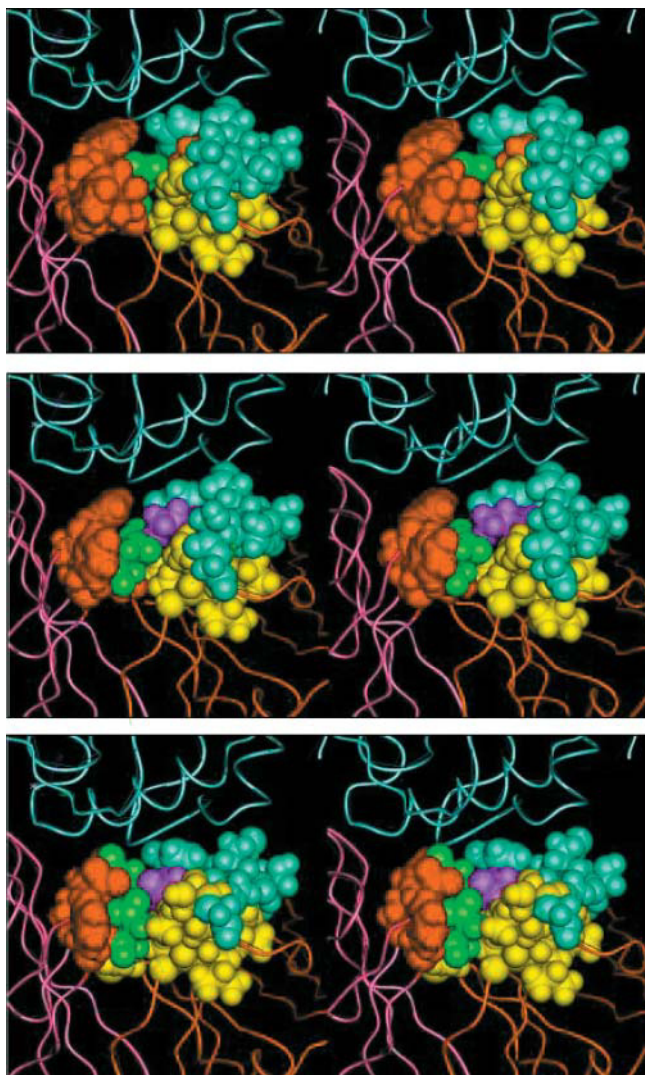
FIGURE 5 Illustration of packing between CDRs L2 and H3. Stereo illustrations depicting the packing interactions between the residues of CDRs L2 and H3 in HH8 (top), HH10 (middle), and HH26 (bottom), CDR residues alone shown in space-filling and rest of the atoms as thin-ribbon representations, respectively. Heavy-chain, light-chain, and HEL are shown in pink, red, and blue, respectively. Polar and hydrophobic residues of CDR L2 are shown in cyan and yellow, respectively, whereas most of the CDR H3 residues are in red. HH8 (top) has threonine at both the positions 49_{Vk} and 101_{VH}, shown in red and green, respectively (whereas they are lysines and aspartic acid, respectively, in both HH10 and HH26), and has hardly any interaction between its CDRs L2 and H3. $K49_{Vk}$ and $D101_{VH}$ residues of HH10 (middle) and H26 (bottom) are shown in magenta and green, respectively. Additionally in HH26, $E96_{VH}$ is also shown in green. HH10 and HH26 have their corresponding CDRs tightly packed due to the electrostatic interaction between their charged residues in L2 and H3. Figures prepared using QUANTA 97.

FIGURE 6 Composite figure of surface representations and intramolecular salt links. In the left panels, the CDR residues alone are shown in molecular surface representations. Surfaces corresponding to hydrophobic, polar, positively-charged, and negatively-charged residues are shown in brown, light blue, dark blue, and magenta, respectively. In the right panels, molecular figures depicting the presence and absence of intramolecular interactions (salt links) are shown. The residues that participate in the intramolecular salt links in HH10 and HH26 (and those corresponding that are not involved in salt links in HH8) are shown in space-filling representation and the rest of the CDR residues in thin-ribbon representation. Molecular surface and intramolecular interactions of HH8 are shown in top-left and top-right panels, respectively; those of HH10 are shown in middle-left and middle-right, respectively; and those of HH26 are shown in bottom-left and bottom-right, respectively. HH8 can be seen to have the largest hydrophobic surface area, whereas HH26 has the largest charged-surface area. Mutation of the two charged residues at positions 49_{Vk} and 101_{VH} in HH8 to threonine precludes most of the salt links that are otherwise present in HH10 and HH26. Substitution of the framework residue at position 94_{VH} from asparagine to arginine leads to formation of extra salt links in HH26.

of CDR-L2 as well. In HH26, the single framework substitution $N94_{VH}R$ leads to the formation of a network of three extra salt bridges, all of the h-h category. Two of these are with residues $E96_{VH}$ and $D101_{VH}$ in H3 and one with residue $D32_{VH}$ in H1 (Fig. 6). HH8 and HH10 have N at

position 94_{VH} (Fig. 1) and hence they do not have these interactions. Residue 34_{VK}, a framework residue according to Chothia numbering and belonging to L1 according to Kabat numbering (Kabat et al., 1991), is hydrogen-bonded to $D96_{VH}$ and $E96_{VH}$ of HH10 and HH26, respectively. This is in addition to the interaction of the later two residues with $K49_{VK}$ of their respective light chains. Notably, HH8 has the $K49T_{VK}$ mutation, and consequently the strong electro-

TABLE 3 Intramolecular salt links observed in the Fv region of HH8, HH10, and HH26

Salt link	HH8	HH10	HH26
R94$_{VH}$–E96$_{VH}$	0 _N94$_{VH}$_,D96$_{VH}$	0 _N94$_{VH}$_,D96$_{VH}$	+ **R94$_{VH}$**,_E96$_{VH}$_
R94$_{VH}$–D101$_{VH}$	0 _N94$_{VH}$_,**T101$_{VH}$**	0 _N94$_{VH}$_,**D101$_{VH}$**	+ **R94$_{VH}$,D101$_{VH}$**
R94$_{VH}$–D32$_{VH}$	0 _N94$_{VH}$_,**D32$_{VH}$**	0 _N94$_{VH}$_,**D32$_{VH}$**	+ **R94$_{VH}$,D32$_{VH}$**
K49$_{V\kappa}$ –D101$_{VH}$	0 **T49$_{V\kappa}$,T101$_{VH}$**	+ **K49$_{V\kappa}$**,_D101$_{VH}$_	+ **K49$_{V\kappa}$,D101$_{VH}$**
K49$_{V\kappa}$–D96$_{VH}$	0 **T49$_{V\kappa}$**,D96$_{VH}$	+ **K49$_{V\kappa}$**,_D96$_{VH}$_	+ **K49$_{V\kappa}$**,_E96$_{VH}$_
H34$_{V\kappa}$–D96$_{VH}$	0 **H34$_{V\kappa}$**,D96$_{VH}$	+ **H34$_{V\kappa}$**,_D96$_{VH}$_	+ **H34$_{V\kappa}$**,_E96$_{VH}$_
R24$_{V\kappa}$–D70$_{V\kappa}$	+ **R24$_{V\kappa}$,D70$_{V\kappa}$**	+ **R24$_{V\kappa}$,D70$_{V\kappa}$**	+ **R24$_{V\kappa}$,D70$_{V\kappa}$**
K64$_{VH}$–D86$_{VH}$	+ **K64$_{VH}$,D86$_{VH}$**	+ **K64$_{VH}$,D86$_{VH}$**	+ **K64$_{VH}$,D86$_{VH}$**

The presence or absence of a given salt link (or ion pair which could participate in electrostatic interactions and/or form a salt link; Sinha et al., 2002) in each antibody is indicated by a + or 0, respectively. Boldface text, _germ-line encoded_; italic text, _D-encoded_; underlined italic text, _codon encoded by joint_; underlined boldface text, _somatic mutation_; and normal text, _unknown_ (the germ-line sequence for this VH gene has not been determined).

static interaction between this residue and D96$_{VH}$ is lacking. D96$_{VH}$ is now shifted, precluding an interaction with H34$_{VK}$.

All the intramolecular salt links present in HH26 are germ-line encoded, whereas HH8 has eliminated almost all of them (excepting the two salt links which are commonly present in all the three antibodies), either by somatic mutations or by codon encoded by joint mechanism (Table 3, this article; see also Lavoie et al., 1999, 1992; Li et al., 2001; Smith-Gill et al., 1987). Half of the salt links present in HH10 are germ-line encoded, whereas the rest have been eliminated through joint and somatic mutation mechanisms (Table 3). Electro-static calculations show that all these intramolecular interactions contribute to the overall free energy of these antibodies and their interactions (Sinha et al., 2002).

Intermolecular interactions in the antibody-antigen complexes

Significant functional differences among these three anti-bodies are correlated with only a limited number of structural

differences (Lavoie et al., 1999) (Tables 3 and 4). The total antigen contact area of the HH8 binding site is 730 Å^2, compared to the values of 750 Å^2 and 760 Å^2 for HH10 and HH26, respectively. The HH8 complex has fewer intermo-lecular hydrogen bonds than either HH10 or HH26. Heavy-chain residues participate in fewer hydrogen bonds with antigen than light-chain residues, mainly due to the substitution of the two tyrosine residues in H2 to phenyl-alanines (Fig. 1). Variation in L3 conformation (Fig. 2, Table 2) results in loss of the hydrogen bond between R21$_{HEL}$ and side-chain Y96$_{VK}$ that is found in HH10-HEL complex. HH8 also has fewer nonbonded contacts with HEL compared to HH10 (Fig. 7, Table 5). Again, the substituted residues Y53$_{VH}$F and Y58$_{VH}$F account for most of the differences (Fig. 3). The van der Waals interaction between the pair of aromatic residues Y33$_{VH}$ and W63$_{HEL}$ is missing in this complex. Only one H-chain residue of HH8 contacts R21$_{HEL}$, compared to three in HH10 (Padlan et al., 1989). As in HH10-HEL complex, a solvent-accessible charged in-teraction is found between D32$_{VH}$ and K97$_{HEL}$.

TABLE 4 Hydrogen bonds between the antibodies and antigen

Lysozyme residue	HH8	HH10	HH26
Light-chain residues			
_Arg_14 O	_Asn_31 ND2	_Asn_31 ND2	_Asn_31 ND2
_Gly_16 O	_Asn_32 ND2	_Asn_32 ND2	_Asn_32 ND2
_Asn_93 OD1	_Gln_53 NE2	_Gln_53 NE2	_Gln_53 NE2
_Asn_93 ND2	_Gln_53 OE1	_Gln_53 OE1	_Gln_53 OE1
_Asn_19 O	_Asn_92 ND2	_Asn_92 ND2	_Asn_92 ND2
_Tyr_20 OH	_Tyr_96 OH	_Tyr_96 OH	_Tyr_96 OH
_Arg_21 N	_Asn_92 O	_Asn_92 O	_Asn_92 O
_Arg_21 NH1		_Tyr_96 OH	_Tyr_96 OH
Heavy-chain residues			
_Arg_73 NH1	_Ser_31 OG	_Thr_30 O, Ser31 OG	_Thr_30 O, Ser31 OG
_Lys_97 NZ	_Asp_32 OD1	_Asp_32 OD1	_Asp_32 OD1, Glu96-OE2
_Lys_97 O	_Tyr_33 OH	_Tyr_33 OH	_Tyr_33 OH
_Arg_21 NH1		_Tyr_50 OH	_Tyr_50 OH
_Ser_100 O		_Tyr_50 OH	_Tyr_50 OH
_Asp_101 OD1	_Asn_56 ND2	_Tyr_53 OH	_Tyr_53 OH
_Gly_102 N		_Tyr_58 OH	_Tyr_58 OH
_Asn_77 OD1			_Arg_94 NH1
Total number of hydrogen bonds	11	16	18

The cutoff distance between the pairs of hydrogen-bonded heavy atoms is 3 Å.
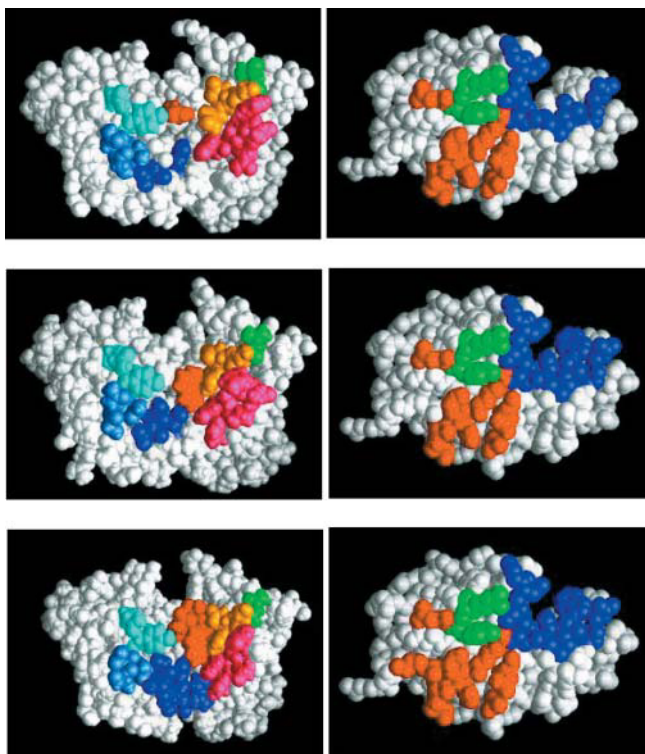
FIGURE 7 Composite figure of contact residues in antibodies and antigen, with figure showing the contact residues of the antibodies and HEL. All atoms are shown in space-filling representations, and those involved in electrostatic and van der Waals interactions alone are shown in color. In the left panels, antibodies are shown. Residues belonging to CDRs L1, L2, and L3 are shown in light blue, cyan, and dark blue, whereas those belonging to CDRs H1, H2, and H3 are shown in orange, magenta, and red, respectively. The framework residues at positions 30_{VH} in all antibodies are shown in green. In right panels, contact residues of HEL are shown; residues contacted by antibody light-chain residues are shown in red; those contacted by heavy-chain residues in dark blue; and those by residues of both chains in green. The top, middle, and bottom panels correspond to HH8-HEL, HH10-HEL, and HH26-HEL complexes, respectively. HH8 can be seen to have the fewest contact residues (which are also scattered), whereas HH26 has the most (and also tightly clustered) contact residues. Correspondingly, the HEL in complex with HH8 has the fewest contact residues, whereas the one in contact with HH26 has the most.

To estimate the extent of packing of the CDRs, the total solvent-accessible surface areas of the CDRs in the absence of HEL was calculated. The binding site of HH26 is the most tightly packed, with a smallest solvent-accessible surface area of 2090 $Å^2$. The corresponding areas for HH8 and HH10 are 2215 $Å^2$ and 2140 $Å^2$, respectively. There are more hydrogen bonds between this antibody and HEL than the other two complexes (Table 4). The increase is a result of both direct and indirect effects of the framework mutation $N94_{VH}R$. Side-chain atom NH1 of $R94_{VH}$ hydrogen bonds to side-chain atom OD1 of $N77_{HEL}$. The salt link between $D32_{VH}$ and $K97_{HEL}$, found in both HH10-HEL and HH8-HEL complexes, is also seen here. In addition, HH26 $E96_{VH}$ is more exposed due to its intramolecular electrostatic interactions with $R94_{VH}$ and $K97_{HEL}$. HH26 has almost

twice the heavy-chain-mediated interactions with (28) compared to HH8 (15).

Modeled complexes of HH8 and HH10 with JQL

The complexes of HH8 and HH10 with Japanese quail lysozyme (JQL) were modeled (Fig. 8) to enable us to understand the fine specificity differences among the three antibodies to antigen mutations (Li et al., 2001; Lavoie et al., 1999, 1992; Sinha et al., 2002). JQL is a natural species variant of HEL with N19K, R21Q, G102V, and N103H mutations. Due to G102V substitution in JQL (PDB code: 2IHL), there is a large local conformational change in the backbone at the C-terminal end of helix containing this (Chitarra et al., 1993). HH8 is able to accommodate the conformational differences of JQL in two ways (Fig. 8): 1), $F58_{VH}$ is turned away from the interface and hence avoids any steric interaction with $D101_{JQL}$, which has shifted relative to the position of $D101_{HEL}$; and 2), it is insensitive to the loss of hydrogen bond with main chain nitrogen at position 102_{JQL} due to the substitution of $F58Y_{VH}$. HH10, on the other hand, is unable to accommodate the structural changes in epitope. HH10 not only suffers a loss of hydrogen bond between its residues $Y58_{VH}$ with main chain N of $G102_{JQL}$, it probably also encounters a severe strain between its residues $Y58_{VH}$ and $D101_{JQL}$. Thus, the higher cross-reactivity of the high affinity HH8 with JQL is modulated at least in part by the higher conformational flexibility of the HH8 combining site. In this case, the conformational flexibility yields greater plasticity, and cross-reactivity is achieved while maintaining high affinity for HEL.

DISCUSSION

The three-dimensional structure of the Fv domains of the two antibodies HH8 and HH26 have been computer-modeled based on the x-ray structure of the highly homologous antibody HH10. The final structures are within 1.2 Å RMS of each other, with small but significant differences in the conformations of their CDRs. Analyses of the antibodies themselves as well as their complexes reveal that these antibodies consistently rank in the same order based on their various chemical and structural properties. Among the three antibodies, HH8 has the most hydrophobic and least charged binding site, whereas HH26 has the least hydrophobic and most charged binding site. HH10 ranks intermediate to the two antibodies. Mutations that increase hydrophobic interactions have been hypothesized to be an important mechanism underlying antibody affinity maturation (Li et al., 2003). HH8 forms the fewest of hydrogen bonds and van der Waals contacts with HEL, whereas HH26 forms the most. HH10 ranks intermediate to the two antibodies. HH8 has the fewest of intramolecular salt bridges whereas HH26 has the most. HH10, once again, ranks between the two. We hypothesize that the presence (or absence) of germ-line

TABLE 5 Nonbonded interactions between HEL and the three antibodies

HEL residues	HH8	HH10	HH26
Light-chain contact residues			
K13			S30
R14	N31	N31	N31
H15	N31	N31	N31
G16	G30, N31	G30, N31, N32	S30, N31, N32
N19	N92	N92	N92
Y20	N32, S91, Y96	N32, S91, N92, Y96	S91, N92, Y96
R21	N92, W94, Y96	N92, Y96	S91, N92, W94, Y96
89	Q53	Q53	Q53
N93	Y50	Y50, Q53	Y50, Q53
K96	Y50	N32, Y50	N32, Y50
Heavy-chain contact residues			
Y20	W95	W95	W95
R21	Y50	Y50, Y58, W95	Y50, Y58, W95
W62		Y53	Y53
W63		Y33, Y53	Y33, Y53
R73	I30, S31	T30, S31	T30, S31
L75	S31	S31, D32	S31, D32, R94
K97	D32, Y33	D32, Y33, W95	D32, Y33, E96, W95
I98	Y33	Y33	Y33
S100	Y50, W95	Y33, Y50, Y58, W95	Y33, Y50, Y58, W95
D101	Y33, S52, F53, S54	Y33, S52, Y53, S54, S56	Y33, S52, Y53, S54, S56
G102	S56	S56, Y58	S56, Y58
Total	29 (LC = 14 + HC = 15)	43 (LC = 17 + HC = 26)	47 (LC = 19 + HC = 28)

Two residues were considered to be involved in nonbonded interaction if the distance between any two pairs of their atoms were at a distance of ≤ 4 Å.

encoded intramolecular salt bridges modulates the flexibility of the antibody-combining side. These properties are summarized in Table 6. From comparison of Table 6 with the functional characteristics in Table 1, it is evident that the structural and functional characteristics are correlated. The high specificity of HH26 is probably mediated by the high number of hydrogen bonds and van der Waals contacts. Computational studies agree with these observations: the HH26 complex exhibits very strong electrostatic interactions, whereas they are weak in HH8 and intermediate in HH10 (Sinha et al., 2002). In contrast, the cross-reactive behavior of HH8 is characterized by fewer of these interactions.

Minimization of template

Among the three antibodies that are being discussed here, the x-ray structure of only HH10 was available at a modest resolution of 3 Å at the time of this study. The variable region of the template (HH10) differs by only 0.85 Å from the recently available structure of a very similar and related antibody HyHEL-63, determined at 2.0 Å resolution (Li et al., 2000). The small RMS difference between these two structures implies that the uncertainty in the structure of HH10 may not be >0.85 Å and hence the HH10-HEL x-ray structure is an appropriate template. Also, the chemical and functional properties of HH8, HH10, and HH26 were consistently correlated among themselves, justifying our choice of HH10 as the template to model the other two.

Despite the high degree of sequence identity, these three antibodies exhibit differences in fine specificity (Table 1).

Since fine specificity might arise from even minor differences in conformations of the side chains, it is important that the positions and conformations of the side chains of the template are known unambiguously. Optimization of the template structure for side-chain packing interactions leads to a significant backbone conformational change in L1. This CDR has been earlier classified to belong to canonical class 2 (Martin and Thornton, 1996); however, after the repacking, the backbone dihedral adopts a slightly different conformation, which now appears closer to canonical class 1 than 2. A higher resolution structure of the template might help to resolve the ambiguity in the classification of the loops. In several earlier instances, refinement of a structure at a higher resolution has led to a revision of classification of the canonical types of its CDRs (Al-Lazikani et al., 1997). In particular, the conformation of L1 in the structure of antibody 4-4-20 was found to conform to the predicted canonical structure after refinement at a higher resolution (Whitlow et al., 1995), which could be interesting in the present context. The backbone dihedral angles (Φ, Ψ) of the residue $Y50_{VK}$ in the template remains in the disallowed region of Ramachandran map even after minimization (68, -52; they are 40, -71 before minimization). Such strained values are also observed in L2 region of the antibody 36-71 (Al-Lazikani et al., 1997).

The x-ray structure of scFvHH10-HEL complex at a resolution of 2.3 Å reveals several side-and main-chain conformational differences from the structure of FabHH10-HEL complex (Kondo et al., 1999). One of the most important backbone differences is found in CDR-H3, where
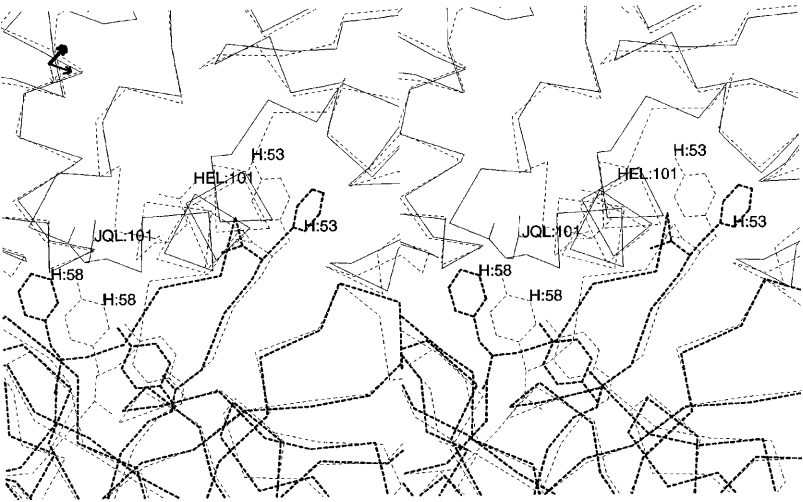
FIGURE 8 Complex of HH8 and HH10 with JQL. Comparison of the model complexes of HH8 and HH10 with JQL (PDB code: 2IHL) and HEL. The structure of JQL (*thin lines*) is superposed on HEL of HH10-HEL complex (*thin dashed lines*). HH8 is shown in thick dashed lines (the HEL in complex with HH8 is not shown for clarity of picture). The residue at position 101_{VH} of JQL has a large shift with respect to its corresponding residue in HEL. HH10 is unable to accommodate this large backbone change in its epitope because its residue $Y58_{VH}$ would have a severe steric clash with the residue 101_{JQL}. However, HH8 can accommodate this large epitope change, because its heavy-chain residue $F58_{VH}$ and the backbone atoms in that local stretch have a different conformation from that of HH10, so as to accommodate this epitope mutation.

the C^α position of residue $D96_{VH}$ has shifted by 2 Å toward HEL and forms a salt bridge with $K97_{HEL}$. Kondo and co-workers also find differences in the packing of heavy and light chains against each other, which they mention is a consequence of the flexibility introduced in the Fv structure by the absence of stabilizing constant domains. In addition, there are differences in affinity between the Fab and scFv complexes (Kondo et al., 1999; Pons et al., 2002). Variations in the packing of heavy and light chains could also affect intermolecular contacts (Tramontano and Lesk, 1992). Hence, the minor differences in intermolecular contacts that are observed in the structure of this scFvHH10-HEL complex may be a consequence of this phenomena arising out of lack of constant domains.

Different antibodies to identical epitopes

It is a well-established fact that antibodies with similar or completely different sequences can be raised against the same antigen or even identical epitope (Schmitter et al., 1990; Goshorn et al., 1991; Kortt et al., 1994; Lescar et al., 1995). The CDRs of such different antibodies might adopt quite similar conformations although may not have identical positions relative to the antigen. A similar phenomena is also observed in this present study, where the three antibodies, as

well as a fourth antibody for which the structure has recently been determined (Li et al., 2000), have been shown to recognize coincident epitopes on HEL (Newman et al., 1992; Lavoie et al., 1999; Li et al., 2001, 2000). The conformations of their CDR-H3 are also quite similar. Subtle differences in their backbone conformations (e.g., CDR-H2 of HH8) likely play significant roles in mediating the specificity differences among them. Comparison of the complexed and uncomplexed structures of HyHEL-63 shows that CDR-H2 of HyHEL-63 displays the largest differences in conformation between the two states (Li et al., 2000), indicative of the inherent flexibility of this CDR. A detailed comparison of the HH10-HEL and HH63-HEL structures is described elsewhere (Li et al., 2000).

Intramolecular salt bridges

Apart from intermolecular interactions, the charged residues in the Fv region form several functionally significant intramolecular salt bridges. Intramolecular salt bridges and hydrogen bonds are known to stabilize protein structures (Horovitz et al., 1990; Vanhove et al., 1995; Takahashi, 1997; Elcock, 1998; Sindelar et al., 1998; Sinha and Smith-Gill, 2002b; Sinha et al., 2001a,b). They have also been observed to have similar roles in antibodies (Parhami-Seren et al.,

TABLE 6 Comparison of structural characteristics of HH8, HH10, and HH26 and their complexes with HEL

Characteristic	HH8	HH10	HH26
Antigen contact area (Å^2)	730	750	760
Antibody contact residues	29	43	47
HEL contact residues	18	20	21
Hydrogen bonds with HEL	11	16	18
Intramolecular salt bridges (Fv)	2	5	8
Binding site charges	Relatively uncharged	Intermediate	Highly charged
Binding site hydrophobicity	Hydrophobic	Intermediate	Not hydrophobic
Conformational flexibility	Relatively flexible	Intermediate	Relatively rigid
Binding mode	Induced-fit	Intermediate	Rigid body ''lock-and-key''

1993; Miyazaki et al., 1997). Effects of such interactions on the structure of the binding sites of HH26 and HH8 are quite evident. HH26, with the most salt bridges, has presumably a rigid and well-compacted binding site, in contrast to the presumably flexible binding site of HH8 which has many fewer salt bridges (Fig. 5). Whereas buried salt bridges destabilize protein structure, those on the surface have a relatively smaller effect on the structure (Schmitt et al., 1999).

Coupled salt bridges forming complex salt-bridge networks contribute to the stability and function of proteins (Horovitz et al., 1990; VanAntwerp and Wittrup, 1998; Sinha and Smith-Gill, 2002a), connect protein subunits (VanAntwerp and Wittrup, 1998), and fine-tune the specific structure of the functional site (Mummert and Voss, 1996). The complex salt-bridge networks found in HH10 and HH26 likely play a similar role (Sinha and Smith-Gill, 2002a). $D101_{VH}$ and $K49_{VK}$, which participate in the network of salt bridges in HH10 and HH26, are not completely on the surface and do not contact the antigen, as can be seen in the x-ray structure of the template (Padlan, 1990). Both these residues as well as residues $E96_{VH}$ and $R94_{VH}$ of HH26 are involved in the formation of the salt-bridge networks interconnecting the CDRs (Sinha et al., unpublished results). Short-term molecular dynamics simulations of these complexes show that the mobility of the CDRs directly correlates with the degree of intramolecular salt bridges networking them (S. Mohan, unpublished results). This implies that these salt bridges can play a major role in mediating the plasticity of the binding site. We hypothesize that these salt bridges of HH10 and HH26 bestow upon their respective binding sites important structural features in terms of providing shape and mediating flexibility. Computational quantification of the energetic contribution of these salt bridges toward the stability of the antibodies (Sinha et al., 2001a,b) are consistent with this prediction (Sinha and Smith-Gill, 2002b).

Determinants of specificity and cross-reactivity in antibody-antigen interactions

The type and extent of intermolecular interactions are quite different in the complexes of these three antibodies with HEL, and clearly correlate with the types of residues present in their respective binding sites. Whereas charged residues in protein-protein interfaces are often responsible for mediating hydrogen bonds and salt bridges (Xu et al., 1997), charge interactions themselves serve as direct sources of specificity in protein-protein interactions (Conte et al., 1999; Pellecchia et al., 1999). These three antibodies also conform to this hypothesis. HH26 with the most charged residues forms the most hydrogen bonds whereas HH8 has the greatest number of hydrophobic residues and forms the fewest hydrogen bonds with HEL. The large number of intermolecular hydrogen bonds of HH26 is one of the likely sources of its

high specificity (Conte et al., 1999; DeLano et al., 2000; Pons et al., 2002). If this is assumed to be true, then a loss of such interactions when it encounters a mutant antigen should be reflected in a significant reduction of association-enthalpic energy. The corresponding fewer hydrogen bonds that HH8 forms should result in a smaller loss of enthalpic energy. Results from isothermal titration calorimetry experiments, performed to measure the association energetics of these antibodies with HEL and JQL, are very supportive of these arguments (Mohan et al., 2000). Relative to their complexes with HEL, the complexes of HH26 and HH8 with JQL exhibit the largest and smallest loss (changes) of enthalpic energy, respectively. The enthalpic loss for HH10-JQL complex is intermediate to the two extremes (Mohan and Willson, unpublished data). Computational studies confirm that among the three complexes, HH8-HEL has the largest hydrophobic contribution to the free energy of binding, and salt bridges in HH8-HEL pay lower desolvation penalties than those in HH10-HEL and HH26-HEL complexes (Sinha et al., 2002). Hydrophobic residues in the interfaces of interacting proteins are believed to mediate stability of the complex, rather than specificity (Janin, 1999; Tsai et al., 1996; Zeder-Lutz et al., 1997; Sinha and Smith-Gill, 2002b). Consistent with this, among the three antibodies, HH8 complexed with native and mutated HEL is the most stable of the three antibodies, as evidenced by low k_d values and slow observed dissociation rates. A similar role can be envisioned for the hydrophobic residues present in the binding site of HH8 when this antibody associates with HEL and other mutant forms. HH8 is predicted to form large nonspecific hydrophobic interactions that could be a source of both cross-reactivity and affinity (Li et al., 2003; Sinha et al., 2002; Mohan et al., unpublished results).

Conformational flexibility is also believed to be yet another source of antibody cross-reactivity (Mian et al., 1991; Jeffrey et al., 1995; Ditzel et al., 1996; Diaw et al., 1997; Sinha and Smith-Gill, 2002b). Studies show that both framework and the CDR regions have a considerable amount of inherent conformational plasticity (Schulze-Gahmen et al., 1993; Stanfield et al., 1993; Arevalo et al., 1994; Holmes and Foote, 1997). However, the structural mechanisms that mediate such topographical complementarity and other conformational flexibility are yet to be defined. Here, for the first time, we propose a mechanism by which intramolecular salt bridges could play a major role in mediating such conformational flexibility of the CDRs. The presence of large number of intramolecular salt bridges in the HH26 renders its CDRs rigid, leading to a "lock-and-key" type of association and making it less adaptable to mutations in epitope. Fewer salt bridges in HH8 allow the CDRs to be more flexible, allowing an induced fit when binding, thus accommodating changes in the epitope. Computation of the relative strength of inter- and intramolecular electrostatic interactions in the three complexes are consistent with this hypothesis (Sinha et al., 2002).

Ample experimental evidence supports these arguments. First, the study of association and dissociation kinetics of these antibodies with HEL and several mutant lysozymes, using the surface plasmon resonance technique, indicate a two-step mode of association, interpreted as an initial encounter followed by a docking or annealing step that could include induced fit (Lipschultz et al., 2002, 2000; Li et al., 2001). The HH8 complex derives the greatest portion of its free energy of binding from the docking step, whereas the corresponding gain for HH26 is the least (Mohan et al., 2003, unpublished results; Li et al., 2001).

Although it is likely that structural rearrangements at the interface are one of several events that could occur during the docking phase and influence the changes in free energy, it nevertheless correlates quite well with our hypothesis that HH8 would be the most likely to undergo conformational rearrangement (due to its flexible binding site), and HH26 to be the least likely to undergo similar change (due to its rigid binding site). Second, changes in configurational entropy, as measured by ITC, is greatest in the complexes of HH8 with both HEL and JQL, smallest in those formed by HH26, and intermediate in those of HH10. This is not possible unless HH8 exhibits an ability to undergo the greatest conformational rearrangement during association, albeit at a cost of large configurational entropic penalty, reflecting its inherent flexibility (Mohan et al., 2000). The opposite of this situation is true of HH26. Both these experimental results support the hypothesis that the three antibodies could exhibit different degrees of flexibilities.

The retention (as in HH26) or elimination (as in HH8) of sequences capable of mediating salt bridges during the process of affinity maturation may well have occurred to obtain the desired structural feature (of having a flexible or rigid binding site), and thus has a functional character of being cross-reactive or specific. Structural differences among the binding sites, which are not necessarily mediated by salt bridges, also have significant direct effects on the ability of these antibodies to cross-react with mutant antigens. This can be illustrated with the models of the complexes of JQL with both HH8 and HH10 (Fig. 8). The conformational changes observed in the CDR-H2 of HH8 as a result of substitution of uncharged residues, and not due to intramolecular salt bridges, is an instance where hydrophobic residues are also likely mediators of cross-reactivity.

Since this study was completed, x-ray crystal structures of HyHEL26 and the chimeric antibody H8L10 complexed with HEL have been determined (Li et al., 2003). The contact interfaces defined by these x-ray structures confirm that the epitopes recognized by all three antibodies are essentially the same. The B-factors, which have been found to generally correlate with motion and flexibility (Micheletti et al., 2002; Smith et al., 2003; Yuan et al., 2003; Eyal et al., 2003; Rees et al., 2000), for all regions of the H8L10 complex were greater than those of the H26 complex, consistent with our hypothesis that HH8 is more flexible than

HH26. Our calculations show that the HH26 model described here and the x-ray crystal structure have high degree of similarity, with an RMS deviation of 1.03 Å (Fig. 9). The residues involved in hydrogen-bond formation are also similar, and there are identical salt bridges shared by the x-ray structure and the model (see Sinha and Smith-Gill, 2002a for a more detailed comparison). Thus, homology-modeling combined with energy minimization of a lower resolution structure (e.g., HH10) can predict a structure of a closely related protein which compares well to its higher resolution x-ray structure. Using a stringently defined criterion of defining salt bridges and hydrogen bonds, we found fewer total salt bridges and H-bonds in the energy-minimized x-ray structure compared to the model (Sinha and Smith-Gill, 2002a; Mohan et al., unpublished results; Sinha et al., 2002). In the same study, the electrostatic interactions or ion pairs not classified as salt bridges in the starting HyHEL63-HEL structure dynamically form salt bridges of good geometry in a large number of MD conformers during the MD simulations (Sinha et al., 2003, unpublished results). Therefore, a complete comparison of the model and x-ray structure will require MD simulation of the dynamic properties. Such a comparison is of significance in evaluating the modeled structures of HH8 as well as HH26, because to date only the chimeric (H8L10) and not the native (HH8) complex has yielded crystals suitable for x-ray analysis (Li et al., 2003). Although many functional properties of H8L10 are similar to those of HH8, there are some significant differences (Lipschultz et al., 2003, unpublished results) and for the immediate future, interpretation of structure-function relationships for the native HH8 antibody will necessarily
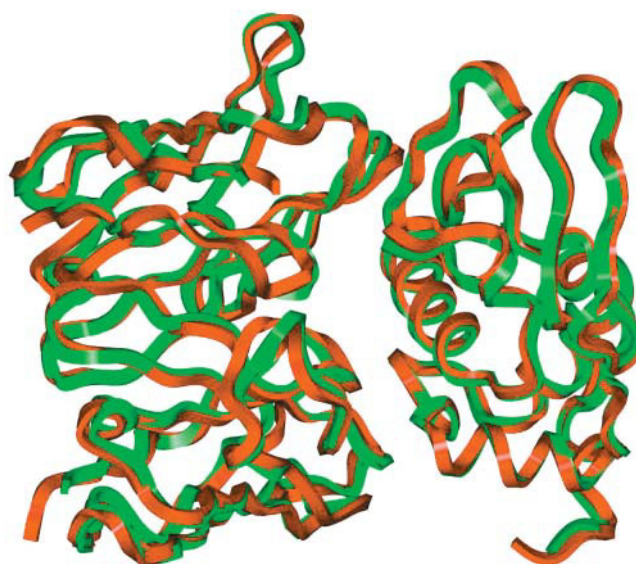

FIGURE 9 Overlay of C^α backbones of the HH26-HEL model and HH26-HEL crystal structure. Crystal structure (Li et al, 2003; PDB accession code 1NDM) is shown in red, and the model in green. Illustration generated using the INSIGHT II package (Accelrys, San Diego, CA).

rely on a homology-modeled structure. Notably, the HH8 model predicts a large shift in the conformation of H2, particularly involving residues *Phe*53 and *Phe*58. This shift is seen in the H8L10 crystal structure and likely adds to the high affinity binding by increasing the contact area of the hydrophobic side chains (Li et al., 2003). In addition, our modeling and molecular dynamics data (Sinha et al., 2002; Sinha and Smith-Gill, 2002a) suggest that the absence of intramolecular salt links in HH8 allows this conformational plasticity, and the even-greater shifting of H2 which is necessary for binding to JQL without a large loss of affinity. We have also noted from the model that the interface of the HH8 complex is the most hydrophobic among the antibodies, and that the nonspecific hydrophobic contacts allow higher affinity binding with HEL mutants, e.g., higher cross-reactivity without loss of affinity or specificity for the unmutated antigen.

CONCLUSIONS

Modeling suggests that the three-dimensional binding site structures of the three antibodies HH8, HH10, and HH26 are quite similar, whereas x-ray crystallography has confirmed that the binding site structures of HH10, HH26, HH63, and the chimeric antibody H8L10 are similar. Comparison of the modeled HH26 and the crystal structure of HH26 establishes that homology-modeling, using as a template a moderate structure, can predict the structure of a higher resolution crystal structure. The specificity and cross-reactivity differences among the antibodies arise from their various numbers of inherent specificity-determining hydrogen bonds and van der Waals contacts as well the abilities of their CDRs to undergo conformational rearrangements that mediate cross-reactivity. The specificity of HH26 correlates with numerous hydrogen bonds in its complex with HEL, and with germ-line encoded intramolecular salt bridges that likely restrain the binding site from assuming alternate conformations to accommodate mutations in epitope. Fewer hydrogen bonds and contacts, more nonspecific hydrophobic contacts, and the absence of intramolecular salt links in HH8 confer conformational flexibility to the binding site, allowing cross-reactivity with mutant antigen. The higher hydrophobic surface area in the interface may at the same time mediate the high affinity of the HH8 complex (Li et al., 2003). HH10 is intermediate in these structural and correlated functional properties. Our results suggest that antibody cross-reactivity correlates with combining site flexibility. Restriction of conformational flexibility in antigen binding has been demonstrated for hapten- and peptide-binding antibodies (Wedemayer et al., 1997; Manivel et al., 2000). In the case of the antibodies described here, higher affinity is not necessarily achieved by more flexibility, but rather, in the case of H10, an intermediate amount of flexibility is optimal, whereas in HH8 higher affinity is accompanied by increased hydrophobicity and increased flexibility (Li et al., 2003).

Thus, affinity maturation may select for high-affinity antibodies with either ''lock-and-key'' preconfigured binding sites, or ''preconfigured flexibility'' through modulation of combining-site flexibility. Detailed NMR analyses of these antibodies would facilitate a more complete understanding of the molecular basis of the specificity and cross-reactivity exhibited by antibodies.

REFERENCES

Abagyan, R., and M. Totrov. 1994. Biased probability Monte Carlo conformational searches and electrostatic calculations for peptides and proteins. *J. Mol. Biol.* 235:983–1002.

Al-Lazikani, B., A. M. Lesk, and C. Chothia. 1997. Standard conformations for the canonical structures of immunoglobulins. *J. Mol. Biol.* 273:927–948.

Anchin, J. M., S. Subramaniam, and D. S. Linthicum. 1991. Binding of the neuroleptic drug haloperidol to a monoclonal antibody: refinement of the binding site molecular model using canonical structures. *J. Mol. Recognit.* 4:7–15.

Arevalo, J. H., C. A. Hassig, E. A. Stura, M. J. Sims, M. J. Taussig, and I. A. Wilson. 1994. Structural analysis of antibody specificity. Detailed comparison of five Fab′-steroid complexes. *J. Mol. Biol.* 241:663–690.

Bahar, I., B. Erman, R. L. Jernigan, A. R. Atilgan, and D. G. Covell. 1999. Collective motions in HIV-1 reverse transcriptase: examination of flexibility and enzyme function. *J. Mol. Biol.* 285:1023–1037.

Barry, M. M., C. D. Mol, W. F. Anderson, and J. S. Lee. 1994. Sequencing and modeling of anti-DNA immunoglobulin Fv domains. Comparison with crystal structures. *J. Biol. Chem.* 269:3623–3632.

Bassolino-Klimas, D., R. E. Bruccoleri, and S. Subramaniam. 1992. Modeling the antigen combining site of an anti-dinitrophenyl antibody, ANO2. *Protein Sci.* 1:1465–1476.

Bentley, G. A. 1996. The crystal structures of complexes formed between lysozyme and antibody fragments. *EXS.* 75:301–319.

Bentley, G. A., T. N. Bhat, G. Boulot, T. Fischmann, J. Navaza, R. J. Poljak, M. M. Riottot, and D. Tello. 1989. Immunochemical and crystallographic studies of antibody D1.3 in its free, antigen-liganded, and idiotope-bound states. *Cold Spring Harbor Symp. Quant. Biol.* 54:239–245.

Brooks, B. R., R. E. Bruccoleri, B. D. Olafson, D. J. States, S. Swaminathan, and M. Karplus. 1983. CHARMM: A program for macromolecular energy, minimization, and dynamics calculations. *J. Comp. Chem.* 4:187–217.

Chitarra, V., P. M. Alzari, G. A. Bentley, T. N. Bhat, J. L. Eisele, A. Houdusse, J. Lescar, H. Souchon, and R. J. Poljak. 1993. Three-dimensional structure of a heteroclitic antigen-antibody cross-reaction complex. *Proc. Natl. Acad. Sci. USA.* 90:7711–7715.

Chothia, C., and A. M. Lesk. 1987. Canonical structures for the hypervariable regions of immunoglobulins. *J. Mol. Biol.* 196:901–917.

Chothia, C., A. M. Lesk, A. Tramontano, M. Levitt, S. J. Smith-Gill, G. Air, S. Sheriff, E. A. Padlan, D. Davies, and W. R. Tulip. 1989. Conformations of immunoglobulin hypervariable regions. *Nature.* 342:877–883.

Conte, L. L., C. Chothia, and J. Janin. 1999. The atomic structure of protein-protein recognition sites. *J. Mol. Biol.* 285:2177–2198.

Davies, D. R., S. Sheriff, and E. A. Padlan. 1988. Antibody-antigen complexes. *J. Biol. Chem.* 263:10541–10544.

DeLano, W. L., M. H. Ultsch, A. M. de Vos, and J. A. Wells. 2000. Convergent solutions to binding at a protein-protein interface. *Science.* 287:1279–1283.

Diaw, L., C. Magnac, O. Pritsch, M. Buckle, P. M. Alzari, and G. Dighiero. 1997. Structural and affinity studies of IgM polyreactive natural autoantibodies. *J. Immunol.* 158:968–976.

Ditzel, H. J., K. Itoh, and D. R. Burton. 1996. Determinants of polyreactivity in a large panel of recombinant human antibodies from HIV-1 infection. *J. Immunol.* 157:739–749.

Elcock, A. H. 1998. The stability of salt bridges at high temperatures: implications for hyperthermophilic proteins. *J. Mol. Biol.* 284:489–502.

Essen, L. O., and A. Skerra. 1994. The de novo design of an antibody combining site. Crystallographic analysis of the VL domain confirms the structural model. *J. Mol. Biol.* 238:226–244.

Eyal, E., R. Najmanovich, M. Edelman, and V. Sobolev. 2003. Protein side-chain rearrangement in regions of point mutations. *Proteins Struct. Funct. Gen.* 50:272–282.

Goshorn, S. C., E. Retzel, and R. Jemmerson. 1991. Common structural features among monoclonal antibodies binding the same antigenic region of cytochrome c. *J. Biol. Chem.* 266:2134–2142.

Holmes, M. S., and J. Foote. 1997. Structural consequences of humanizing an antibody. *J. Immunol.* 158:2192–2201.

Horovitz, A., L. Serrano, B. Avron, M. Bycroft, and A. R. Fersht. 1990. Strength and co-operativity of contributions of surface salt bridges to protein stability. *J. Mol. Biol.* 216:1031–1044.

Janin, J. 1999. Wet and dry interfaces: the role of solvent in protein-protein and protein-DNA recognition. *Struct. Fold. Des.* 7:R277–R279.

Jeffrey, P. D., J. F. Schildbach, C. Y. Chang, P. H. Kussie, M. N. Margolies, and S. Sheriff. 1995. Structure and specificity of the anti-digoxin antibody 40–50. *J. Mol. Biol.* 248:344–360.

Kabat, E. A., T. T. Wu, H. M. Perry, K. S. Gottesman, and C. Foeller. 1991. Sequences of Proteins of Immunological Interest. U.S. Department of Health, Education, and Welfare, NIH, Bethesda, MD.

Kam-Morgan, L. N., T. B. Lavoie, S. J. Smith-Gill, and J. F. Kirsch. 1993. Site-directed mutagenesis in analysis of protein-protein interactions. *Methods Enzymol.* 224:503–516.

Kondo, H., M. Shiroishi, M. Matsushima, K. Tsumoto, and I. Kumagai. 1999. Crystal structure of anti-hen egg white lysozyme antibody (HyHEL-10) Fv-antigen complex. Local structural changes in the protein antigen and water-mediated interactions of Fv-antigen and light chain-heavy chain interfaces. *J. Biol. Chem.* 274:27623–27631.

Kortt, A. A., R. L. Malby, J. B. Caldwell, L. C. Gruen, N. Ivancic, M. C. Lawrence, G. J. Howlett, R. G. Webster, P. J. Hudson, and P. M. Colman. 1994. Recombinant anti-sialidase single-chain variable fragment antibody. Characterization, formation of dimer and higher-molecular-mass multimers and the solution of the crystal structure of the single-chain variable fragment/sialidase complex. *Eur. J. Biochem.* 221:151–157.

Lavoie, T. B., W. N. Drohan, and S. J. Smith-Gill. 1992. Experimental analysis by site-directed mutagenesis of somatic mutation effects on affinity and fine specificity in antibodies specific for lysozyme. *J. Immunol.* 148:503–513.

Lavoie, T. B., S. Mohan, C. A. Lipschultz, J. C. Grivel, Y. Li, C. R. Mainhart, L. N. W. Kam-Morgan, W. N. Drohan, and S. J. Smith-Gill. 1999. Structural differences among monoclonal antibodies with distinct fine specificities and kinetic properties. *Mol. Immunol.* 36:1189–1205.

Lee, C., and M. Levitt. 1991. Accurate prediction of the stability and activity effects of site-directed mutagenesis on a protein core. *Nature.* 352:448–451.

Lee, C., and S. Subbiah. 1991. Prediction of protein side-chain conformation by packing optimization. *J. Mol. Biol.* 217:373–388.

Lescar, J., M. Pellegrini, H. Souchon, D. Tello, R. J. Poljak, N. Peterson, N. Greene, and P. M. Alazari. 1995. Crystal structure of a cross-reaction complex between Fab F9.13.7 and guinea fowl lysozyme. *J. Biol. Chem.* 270:18067–18076.

Levitt, M. 1983. Protein folding by restrained energy minimization and molecular dynamics. *J. Mol. Biol.* 170:723–764.

Levitt, M. 1992. Accurate modeling of protein conformation by automatic segment matching. *J. Mol. Biol.* 226:507–533.

Li, Y. L., H. M. Li, S. J. Smith-Gill, and R. A. Mariuzza. 2000. Three-dimensional structures of the free and antigen-bound Fab from monoclonal antilysozyme antibody HyHEL-63. *Biochemistry.* 39:6296–6309.

Li, Y. L., H. M. Li, F. Yang, S. J. Smith-Gill, and R. A. Mariuzza. 2003. X-ray snapshots of the maturation of an antibody response to a protein antigen. *Nat. Struct. Biol.* 10:482–488.

Li, Y. L., C. A. Lipschultz, S. Mohan, and S. J. Smith-Gill. 2001. Mutations of an epitope hot-spot residue alter rate limiting steps of antigen-antibody protein-protein associations. *Biochemistry.* 40:2011–2022.

Lipschultz, C. A., Y. L. Li, and S. Smith-Gill. 2000. Experimental design for analysis of complex kinetics using surface plasmon resonance. *Meth. Comp. Meth. Enzymol.* 20:310–318.

Lipschultz, C. A., A. Yee, S. Mohan, Y. L. Li, and S. J. Smith-Gill. 2002. Temperature differentially affects encounter and docking thermodynamics of antibody-antigen association. *J. Mol. Recognit.* 15:44–52.

MacCallum, R. M., A. C. Martin, and J. M. Thornton. 1996. Antibody-antigen interactions: contact analysis and binding site topography. *J. Mol. Biol.* 262:732–745.

Manivel, V., N. C. Sahoo, D. M. Salunke, and K. V. S. Rao. 2000. Maturation of an antibody response is governed by modulations in flexibility of the antigen-combining site. *Immunity.* 13:611–620.

Martin, A. C. and J. M. Thornton. 1996. Structural families in loops of homologous proteins: automatic classification, modelling and application to antibodies. *J. Mol. Biol.* 263:800–815.

Mas, M. T., K. C. Smith, D. L. Yarmush, K. Aisaka, and R. M. Fine. 1992. Modeling the anti-CEA antibody combining site by homology and conformational search. *Proteins.* 14:483–498.

Mian, I. S., A. R. Bradwell, and A. J. Olson. 1991. Structure, function and properties of antibody binding sites. *J. Mol. Biol.* 217:133–151.

Micheletti, C., G. Lattanzi, and A. Maritan. 2002. Elastic properties of proteins: insight on the folding process and evolutionary selection of native structures. *J. Mol. Biol.* 321:909–921.

Miller, C. E., L. A. Mulard, E. A. Padlan, and C. P. Glaudemans. 1998. Binding of modified fragments of the *Shigella dysenteriae* type 1 O-specific polysaccharide to monoclonal IgM 3707 E9 and docking of the immunodeterminant to its modeled Fv. *Carbohydr. Res.* 309:219–226.

Miyazaki, S., J. Shimura, S. Hirose, R. Sanokawa, H. Tsurui, M. Wakiya, H. Sugawara, and T. Shirai. 1997. Is structural flexibility of antigen-binding loops involved in the affinity maturation of anti-DNA antibodies? *Int. Immunol.* 9:771–777.

Mohan, S., H. Uehara, S. J. Smith-Gill, and R. C. Willson. 2000. Association energetics of cross-reactive and specific antibodies. *Biophys. J.* 78:39A.

Mummert, M. E., and E. W. J. Voss. 1996. Transition-state theory and secondary forces in antigen-antibody complexes. *Biochemistry.* 35:8187–8192.

Neri, D., M. Momo, T. Prospero, and G. Winter. 1995. High-affinity antigen binding by chelating recombinant antibodies (CRAbs). *J. Mol. Biol.* 246:367–373.

Newman, M. A., C. R. Mainhart, C. P. Mallett, T. B. Lavoie, and S. J. Smith-Gill. 1992. Patterns of antibody specificity during the BALB/c immune response to hen egg-white lysozyme. *J. Immunol.* 149:3260–3272.

Novotny, J., and K. Sharp. 1992. Electrostatic fields in antibodies and antibody/antigen complexes. *Prog. Biophys. Mol. Biol.* 58:203–224.

Orlandini, M., A. Santucci, A. Tramontano, P. Neri, and S. Oliviero. 1994. Cloning, characterization, and modeling of a monoclonal anti-human transferrin antibody that competes with the transferrin receptor. *Protein Sci.* 3:1476–1484.

Padlan, E. A. 1990. On the nature of antibody combining sites: unusual structural features that may confer on these sites an enhanced capacity for binding ligands. *Proteins.* 7:112–124.

Padlan, E. A., E. W. Silverton, S. Sheriff, G. H. Cohen, S. J. Smith-Gill, and D. R. Davies. 1989. Structure of an antibody-antigen complex: crystal structure of the HyHEL-10 Fab-lysozyme complex. *Proc. Natl. Acad. Sci. USA.* 86:5938–5942.

Parhami-Seren, B., P. H. Kussie, R. K. Strong, and M. N. Margolies. 1993. Conservation of binding site geometry among *p*-azophenylarsonate-specific antibodies. *J. Immunol.* 150:1829–1837.

Pellecchia, M., P. Sebbel, U. Hermanns, K. Wuthrich, and R. Glockshuber. 1999. Pilus chaperone FimC-adhesin FimH interactions mapped by TROSY-NMR. *Nat. Struct. Biol.* 6:336–339.

Pons, J., A. Rajpal, and J. F. Kirsch. 1999. Energetic analysis of an antigen/antibody interface: alanine scanning mutagenesis and double mutant cycles on the HyHEL-10/lysozyme interaction. *Protein Sci.* 8:958–968.

Pons, J., J. R. Stratton, and J. F. Kirsch. 2002. How do two unrelated antibodies, HyHEL-10 and F9.13.7, recognize the same epitope of hen egg-white lysozyme? *Protein Sci.* 11:2308–2315.

Rajpal, A., M. G. Taylor, and J. F. Kirsch. 1998. Quantitative evaluation of the chicken lysozyme epitope in the HyHEL-10 Fab complex: free energies and kinetics. *Protein Sci.* 7:1868–1874.

Rees, B., G. Webster, M. Delarue, M. Boeglin, and D. Moras. 2000. Aspartyl tRNA-synthetase from *Escherichia coli*: flexibility and adaptability to the substrates. *J. Mol. Biol.* 299:1157–1164.

Schiweck, W. and A. Skerra. 1997. The rational construction of an antibody against cystatin: lessons from the crystal structure of an artificial Fab fragment. *J. Mol. Biol.* 268:934–951.

Schmitt, L., J. J. Boniface, M. M. Davis, and H. M. McConnell. 1999. Conformational isomers of a class II MHC-peptide complex in solution. *J. Mol. Biol.* 286:207–218.

Schmitter, D., O. Poch, G. Zeder, G. F. Heinrich, H. P. Kocher, V. F. Quesniaux, and M. H. Van Regenmortel. 1990. Analysis of the structural diversity of monoclonal antibodies to cyclosporine. *Mol. Immunol.* 27:1029–1038.

Schulze-Gahmen, U., J. M. Rini, and I. A. Wilson. 1993. Detailed analysis of the free and bound conformations of an antibody. X-ray structures of Fab 17/9 and three different Fab-peptide complexes. *J. Mol. Biol.* 234:1098–1118.

Shick, K. A., K. A. Xavier, A. Rajpal, S. J. Smith-Gill, and R. C. Willson. 1997. Association of the anti-hen egg lysozyme antibody HyHEL-5 with avian species variant and mutant lysozymes. *Biochim. Biophys. Acta.* 1340:205–214.

Sindelar, C. V., Z. S. Hendsch, and B. Tidor. 1998. Effects of salt bridges on protein structure and design. *Protein Sci.* 7:1898–1914.

Sinha, N., S. Mohan, C. A. Lipschultz, and S. J. Smith-Gill. 2002. Differences in electrostatic properties at antibody-antigen binding sites: implications for specificity and cross-reactivity. *Biophys. J.* 83:2946–2968.

Sinha, N., and S. J. Smith-Gill. 2002a. Electrostatics in protein binding and function. *Curr. Protein Peptide Sci.* 3:601–614.

Sinha, N., and S. J. Smith-Gill. 2002b. Protein structure to function via dynamics. *Protein Peptide Lett.* 9:367–377.

Sinha, N., C. J. Tsai, and R. Nussinov. 2001a. A proposed structural model for amyloid fibril elongation: domain swapping forms an interdigitating β-structure polymer. *Protein Eng.* 14:93–103.

Sinha, N., C. J. Tsai, and R. Nussinov. 2001b. Building blocks, hinge-bending motions and protein topology. *J. Biomol. Struct. Dyn.* 19:369–380.

Smith-Gill, S. J. 1994. Protein epitopes: functional vs. structural definitions. *Res. Immunol.* 145:67–70.

Smith-Gill, S. J. 1996. Molecular recognition of lysozyme by monoclonal antibodies. *In* Lysozymes: Model Enzymes in Biochemistry. P. Jolles, editor. Berkhauser Verlag, Basel, Switzerland. 277–300.

Smith-Gill, S. J., T. B. Lavoie, and C. R. Mainhart. 1984. Antigenic regions defined by monoclonal antibodies correspond to structural domains of avian lysozyme. *J. Immunol.* 133:384–393.

Smith-Gill, S. J., C. Mainhart, T. B. Lavoie, R. J. Feldmann, W. Drohan, and B. R. Brooks. 1987. A three-dimensional model of an anti-lysozyme antibody. *J. Mol. Biol.* 194:713–724.

Smith, D. K., P. Radivojac, Z. Obradovic, A. K. Dunker, and G. Zhu. 2003. Improved amino acid flexibility parameters. *Protein Sci.* 12:1060–1072.

Stanfield, R. L., M. Takimoto-Kamimura, J. M. Rini, A. T. Profy, and I. A. Wilson. 1993. Major antigen-induced domain rearrangements in an antibody. *Structure.* 1:83–93.

Takahashi, T. 1997. Significant role of electrostatic interactions for stabilization of protein assemblies. *Adv. Biophys.* 34:41–54.

Tanner, J. J., L. J. Nell, and J. A. McCammon. 1992. Anti-insulin antibody structure and conformation. II. Molecular dynamics with explicit solvent. *Biopolymers.* 32:23–32.

Tenette-Souaille, C., and J. C. Smith. 1998. Structural modeling of the complex between an acetylcholine receptor- mimicking antibody and its snake toxin antigen. *Proteins.* 30:249–263.

Tenette, C., F. Ducancel, and J. C. Smith. 1996. Structural model of the anti-snake-toxin antibody, M$^\alpha$ 2,3. *Proteins.* 26:9–31.

Tramontano, A., and A. M. Lesk. 1992. Common features of the conformations of antigen-binding loops in immunoglobulins and application to modeling loop conformations. *Proteins.* 13:231–245.

Tsai, C. J., S. L. Lin, H. J. Wolfson, and R. Nussinov. 1996. Protein-protein interfaces: architectures and interactions in protein-protein interfaces and in protein cores. Their similarities and differences. *Crit. Rev. Biochem. Mol. Biol.* 31:127–152.

Tsumoto, K., K. Ogasahara, Y. Ueda, K. Watanabe, K. Yutani, and I. Kumagai. 1996. Role of salt bridge formation in antigen-antibody interaction. Entropic contribution to the complex between hen egg white lysozyme and its monoclonal antibody HyHEL10. *J. Biol. Chem.* 271:32612–32616.

VanAntwerp, J. J., and K. D. Wittrup. 1998. Thermodynamic character-ization of affinity maturation: the D1.3 antibody and a higher-affinity mutant. *J. Mol. Recognit.* 11:10–13.

Vanhove, M., S. Houba, J. Motte-Brasseur, and J. M. Frere. 1995. Probing the determinants of protein stability: comparison of class A β-lactamases. *Biochem. J.* 308:859–864.

Walls, P. H., and M. J. Sternberg. 1992. New algorithm to model protein-protein recognition based on surface complementarity. Applications to antibody-antigen docking. *J. Mol. Biol.* 228:277–297.

Wedemayer, G. J., P. A. Patten, L. H. Wang, P. G. Schultz, and R. C. Stevens. 1997. Structural insights into the evolution of an antibody combining site. *Science.* 276:1665–1669. (See also comments in published erratum, *Science*, 1997, 277:1423.)

Whitlow, M., A. J. Howard, J. F. Wood, E. W. J. Voss, and K. D. Hardman. 1995. 1.85 Å structure of anti-fluorescein 4–4-20 Fab. *Protein Eng.* 8:749–761.

Wilson, I. A., R. L. Stanfield, J. M. Rini, J. H. Arevalo, U. Schulze-Gahmen, D. H. Fremont, and E. A. Stura. 1991. Structural aspects of antibodies and antibody-antigen complexes. *CIBA Found. Symp.* 159:13–39.

Wu, T. T., G. Johnson, and E. A. Kabat. 1993. Length distribution of CDRH3 in antibodies. *Proteins.* 16:1–7.

Xu, D., C. J. Tsai, and R. Nussinov. 1997. Hydrogen bonds and salt bridges across protein-protein interfaces. *Protein Eng.* 10:999–1012.

Yuan, Z., J. Zhao, and Z. X. Wang. 2003. Flexibility analysis of enzyme active sites by crystallographic temperature factors. *Protein Eng.* 16:109–114.

Zeder-Lutz, G., E. Zuber, J. Witz, and M. H. Van Regenmortel. 1997. Thermodynamic analysis of antigen-antibody binding using biosensor measurements at different temperatures. *Anal. Biochem.* 246:123–132.